Nuclear Engineering and Technology 49 (2017) 1636–1644

Contents lists available at ScienceDirect

Nuclear Engineering and Technology

journal homepage: www.elsevier.com/locate/net

Original Article

Effect of a chemical reaction on magnetohydrodynamic (MHD) stagnation point flow of Walters-B nanofluid with newtonian heat and mass conditions

Sajid Qayyum [a, *], Tasawar Hayat [a, b], Sabir A. Shehzad [c], Ahmed Alsaedi [b]

[a] Department of Mathematics, Quaid-I-Azam University 45320, Islamabad 44000, Pakistan
[b] Nonlinear Analysis and Applied Mathematics (NAAM) Research Group, Faculty of Science, King Abdulaziz University, P.O. Box 80207, Jeddah 21589, Saudi Arabia
[c] Department of Mathematics, COMSATS Institute of Information Technology, Sahiwal 57000, Pakistan

ARTICLE INFO

Article history:
Received 17 May 2017
Received in revised form
17 July 2017
Accepted 25 July 2017
Available online 14 September 2017

Keywords:
Chemical Reaction
Magnetohydrodynamic (MHD)
Newtonian Conditions
Stagnation Point Flow
Thermal Radiation
Walter-B Nanofluid

ABSTRACT

The main purpose of this article is to describe the magnetohydrodynamic stagnation point flow of Walter-B nanofluid over a stretching sheet. The phenomena of heat and mass transfer are based on the involvement of thermal radiation and chemical reaction. Characteristics of Newtonian heating are given special attention. The Brownian motion and thermophoresis models are introduced in the temperature and concentration expressions. Appropriate variables are implemented for the transformation of partial differential frameworks into sets of ordinary differential equations. Plots for velocity, temperature, and nanoparticle concentration are displayed and analyzed for governing parameters. The skin friction coefficient and local Nusselt and Sherwood numbers are studied using numerical values. The temperature and heat transfer rate are enhanced within the frame of the thermal conjugate parameter.

1. Introduction

A “nanofluid” is a liquid in which solid particles of dimensions less than 100 nm are dispersed. In general, nanoliquids are a mixture of nanoparticles and base liquids. In nature, various types of base liquids exist, namely oils, water, lubricants, polymeric solutions, bio-fluids, and organic liquids (e.g., refrigerants and ethylene glycol). Recent advancements on this topic clearly show that nanoliquids have the capability of improving the thermal performance and thermal conductivity of ordinary liquids. The improvement in heat transfer performance greatly depends on particle shape, the type of material, and the size of the submerged particles. Recent modern technology clearly demonstrates that nanofluids have a potential role in the manufacturing of cars, airplanes, microreactors, micromachines, and so on. The unique chemical and physical features of nanosized material further enhances the application of nanoliquids in industrial processes, such as melt-spinning, manufacture of rubber and plastic sheets, drying and cooling of papers, petroleum reservoirs, extrusion of plastic materials, nuclear reactors, rotors of gas turbines, air cleaning machines, electronic devices, and medical equipment. Choi [1] developed the model of submersion of tiny solid particles in an ordinary liquid. He performed the experimental analysis on nanoliquids and found that the involvement of solid particles in base liquids is the best method to enhance thermal performance. Buongiorno [2] found that the Brownian movement of nanomaterials is one of the key parameters that enhances the thermal conductivity of ordinary liquids. A large amount of research on the mechanism of nanofluids under various aspects and geometries has been carried out. Some relevant recent works can be seen in references [3–18].

The importance of non-Newtonian liquids in industry and technology is increasing day by day due to their diverse practical applications. A few examples of these practical applications are clay coatings, exotic lubricants, paints, certain oils, colloidal suspensions, cosmetic and food products, etc. The diversity of these liquids in physical nature is a major issue because scientists are unable to derive a single mathematical relationship that incorporates the

* Corresponding author.
E-mail address: sajidqayyum94@gmail.com (S. Qayyum).

https://doi.org/10.1016/j.net.2017.07.028

nature of all non-Newtonian liquids. Therefore, various non-Newtonian fluid models, using the nature of individual liquids, have been developed in the past. Here, we consider Walter's liquid B model [19], which predicts the nature of different polymeric fluids appearing in chemical engineering and biotechnology. Nandeppanavar et al. [20] described the features of Walter's liquid B fluid over a moving permeable surface under the elastic deformation effect. Hakeem et al. [21] addressed the heat radiative flow of Walter's liquid B model through nonuniform heat absorption and generation. The characteristics of heat transport in Walter's liquid B fluid via the Robin condition have been explored by Hayat et al. [22]. Javed et al. [23] discussed peristaltic activity of Walter's fluid B model through momentum and temperature slip conditions. Hayat et al. [24] studied the magnetohydrodynamic (MHD) nonlinear convective flow of the Walters-B magneto nanofluid towards a variable thickness sheet in the presence of heat generation/absorption.

In industrial processes, proper knowledge of heat transport is essential to achieving the best quality product. The processes of heating are generally classified into four types. One type of heating process is known as "Newtonian heating". In this category, the heat is transferred to the convective fluid through the bounding surface of a specified heat capacity. The phenomenon of Newtonian heating has potential applications in the petroleum industry, conjugate heat transport, heat exchangers, thermal energy storage, nuclear turbines, etc. The impact of Newtonian heating and Navier slip in time-dependent hydromagnetic fluid flow has been reported by Makinde [25]. Shehzad et al. [26] provided the analysis of three-dimensional Jeffrey fluid flow through the Newtonian heating condition. Ramzan et al. [27] developed the homotopic solutions of three-dimensional Oldroyd B liquid flow under the Newtonian heating process. The nonlinear stretched flow phenomenon of the Jeffrey liquid via Newtonian heating has been described by Hayat et al. [28].

In this attempt, our focus is to evaluate the interaction of Newtonian heat and mass processes in Walters-B fluid bounded by a moving surface. In past investigations only the Newtonian heating of heat transfer has been used to examine the features of different fluid models under various aspects and flow geometries. Here we developed the Newtonian mass condition for stretching flow behavior of the non-Newtonian liquid. Further, we considered Brownian motion and thermophoresis. A thermal stagnation point flow is considered. The boundary layer expressions of the physical problem are developed. The analytical procedure via the homotopic method [29–40] is carried out to elaborate on the solutions of dimensionless quantities. Graphs and numerical tables are generated to address the nature of arising dimensionless parameters.

2. Mathematical modeling

Consider the steady two-dimensional stagnation point flow of Walters-B nanofluid towards an impermeable stretching sheet. The flow is induced, due to the stretching surface at $y = 0$, whereas the fluid occupies in domain $y \geqslant 0$. It is assumed that stretching velocity of the sheet is $u_w(x) = ax$ and the velocity of the ambient flow is $u_e(x) = cx$, where a and c denote positive constants. The strength of a uniform magnetic field B_0 is utilized in the y direction (see Fig. 1). Newtonian heating models for temperature and concentration are employed. Thermal radiation and chemical reaction are present. Flow analysis further consists of Brownian motion and thermophoresis. The continuity, momentum, energy, and concentration expressions after boundary layer approximations $[u = O(1), x = O(1), v = O(\delta), y = O(\delta)]$ are

$$\frac{\partial u}{\partial x} + \frac{\partial v}{\partial y} = 0, \tag{1}$$

$$u\frac{\partial u}{\partial x} + v\frac{\partial u}{\partial y} = u_e(x)\frac{\partial u_e(x)}{\partial x} + \nu\frac{\partial^2 u}{\partial y^2} - \Omega\left[u\frac{\partial^3 u}{\partial x \partial y^2} + v\frac{\partial^3 u}{\partial y^3} + \frac{\partial u}{\partial x}\frac{\partial^2 u}{\partial y^2} - \frac{\partial u}{\partial y}\frac{\partial^2 u}{\partial x \partial y}\right] - \frac{\sigma B_0^2}{\rho}[u - u_e(x)], \tag{2}$$

$$u\frac{\partial T}{\partial x} + v\frac{\partial T}{\partial y} = \frac{k_f}{(\rho c_p)_f}\left(\frac{\partial^2 T}{\partial y^2}\right) + \tau D_B\left(\frac{\partial T}{\partial y}\frac{\partial C}{\partial y}\right) + \frac{\tau D_T}{T_\infty}\left(\frac{\partial T}{\partial y}\right)^2 - \frac{1}{(\rho c_p)_f}\frac{\partial q_r}{\partial y}, \tag{3}$$

$$u\frac{\partial C}{\partial x} + v\frac{\partial C}{\partial y} = D_B\left(\frac{\partial^2 C}{\partial y^2}\right) + \frac{D_T}{T_\infty}\left(\frac{\partial^2 T}{\partial y^2}\right) - k^*(C - C_\infty), \tag{4}$$

with

$$u = u_w(x) = ax,\ v = 0, \frac{\partial T}{\partial y} = -h_t T, \frac{\partial C}{\partial y} = -h_c C \quad \text{at} \quad y = 0,$$
$$u = u_e(x) = cx, T \to T_\infty, C \to C_\infty \quad \text{as} \quad y \to \infty. \tag{5}$$

Here, parallel to the x-and y axes, the velocity components are denoted by (u, v) $\nu = (\mu/\rho)_f$ represents kinematic viscosity, Ω is the elastic parameter, σ is the electrical conductivity, ρ_f represents fluid density, $(c_p)_f$ is the fluid heat capacity, ρ_p is the particle density, $(c_p)_p$ is the particle heat capacity, k_f represents thermal conductivity, q_r denotes the radiative heat flux, $\tau = (\rho c_p)_p/(\rho c_p)_f$ is the capacity ratio, D_B is the Brownian diffusion coefficient, D_T represents the thermophoretic diffusion coefficient, T is the fluid temperature, C is the fluid concentration, T_∞ denotes the ambient fluid temperature, C_∞ is the nanoparticle concentration far away from the surface, k^* represents the reaction rate, where $k^* > 0$ corresponds to destructive and $k^* < 0$ to generative reactions, h_t is the heat transfer coefficient, h_c denotes the mass diffusion coefficient, a is the stretching rate, and c is the rate of free stream velocity.

The Rosseland relation for radiative heat flux q_r is [40].

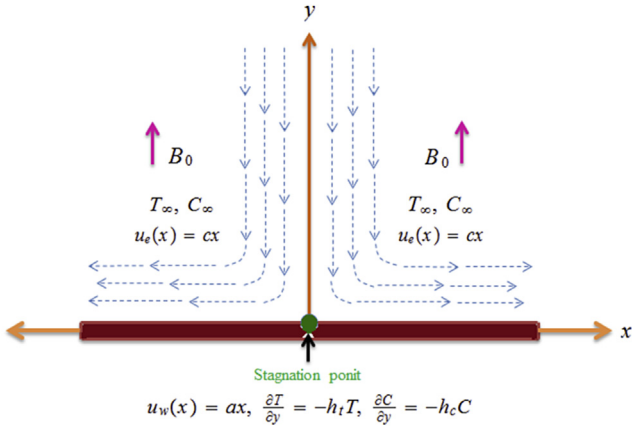

Fig. 1. Flow configuration and coordinate system.

$$q_r = -\frac{4\sigma^*}{3k^*}\frac{\partial T^4}{\partial y}, \tag{6}$$

where σ^* denotes the Stefan–Boltzmann constant and k^* shows the mean absorption coefficient. We assume that the difference in the temperature in the flow analysis is such that the term T^4 may be expanded in a Taylor series. Hence, expanding T^4 about T_∞ and omitting higher terms we obtain

$$T^4 \cong 4T_\infty^3 T - 3T_\infty^4. \tag{7}$$

Thus using Eq. (7) in Eq. (6), we get

$$q_r = -\frac{16\sigma^* T_\infty^3}{3k^*}\frac{\partial T}{\partial y}. \tag{8}$$

Now Eqs. (3) and (8) yield

$$u\frac{\partial T}{\partial x} + v\frac{\partial T}{\partial y} = \frac{k_f}{(\rho c_p)_f}\left(\frac{\partial^2 T}{\partial y^2}\right) + \tau D_B\left(\frac{\partial T}{\partial y}\frac{\partial C}{\partial y}\right) + \frac{\tau D_T}{T_\infty}\left(\frac{\partial T}{\partial y}\right)^2 + \frac{1}{(\rho c_p)_f}\frac{16\sigma^* T_\infty^3}{3k^*}\frac{\partial^2 T}{\partial y^2}. \tag{9}$$

Considering

$$\eta = \sqrt{\frac{a}{\nu}}y, \quad \theta(\eta) = \frac{T - T_\infty}{T_\infty}, \quad \phi(\eta) = \frac{C - C_\infty}{C_\infty}, \\ u = axf'(\eta), \quad v = -\sqrt{a\nu}f(\eta), \quad \psi(\eta) = \sqrt{a\nu}xf(\eta), \tag{10}$$

Eq. (1) is trivially satisfied and other equations yield

$$f''' + ff'' - \left(f'\right)^2 + \alpha\left(f''^2 - 2f'f''' + ff^{iv}\right) - H_a^2\left(f' - A^*\right) + (A^*)^2 = 0, \tag{11}$$

$$\left(1 + \frac{4}{3}R\right)\theta'' + \Pr f\theta' + \Pr N_b\theta'\phi' + \Pr N_t\left(\theta'\right)^2 = 0, \tag{12}$$

$$\phi'' + Sc\left(f\phi' - \gamma\phi\right) + \frac{N_t}{N_b}\theta'' = 0, \tag{13}$$

$$f'(\eta) = 1, \quad f(\eta) = 0, \quad \theta'(\eta) = -B_t[1 + \theta(\eta)], \\ \phi'(\eta) = -B_c[1 + \phi(\eta)] \quad \text{at} \quad \eta = 0, \\ f'(\eta) = A^*, \quad \theta(\eta) = 0, \quad \phi(\eta) = 0 \quad \text{as} \quad \eta \to \infty, \tag{14}$$

in which prime denotes differentiation with respect to η, α is the viscoelastic parameter, H_a denotes the magnetic parameter/Hartman number, A^* represents the ratio of rates, R is the radiation parameter, Pr denotes the Prandtl number, N_b is the Brownian motion parameter, N_t is the thermophoresis parameter, Sc denotes the Schmidt number, γ is the chemical reaction parameter, and B_t and B_c represent the thermal and solutal conjugate parameters. Definitions of the involved parameters are

$$\alpha = \frac{\Omega a}{\nu}, \quad H_a = \frac{\sigma B_0^2}{\rho a}, \quad A = \frac{c}{a}, \quad R = \frac{4\sigma^* T_\infty^3}{k_f k^*}, \quad \Pr = \frac{\mu c_p}{k_f}, \quad N_b = \frac{\tau D_B}{\nu}, \\ N_t = \frac{\tau D_T}{\nu T_\infty}, \quad Sc = \frac{\nu}{D_B}, \quad \gamma = \frac{k^*}{a}, \quad B_t = h_t\sqrt{\frac{\nu}{a}}, \quad B_c = h_c\sqrt{\frac{\nu}{a}}. \tag{15}$$

It should be noted that $\alpha = 0$ in Eq. (11) yields a Newtonian fluid.

The skin friction coefficient C_{f_x} and local Nussult Nu_x and Sherwood Sh_x numbers are

$$C_{f_x} = \frac{\tau_w}{\frac{1}{2}\rho u_w^2}, \quad Nu_x = \frac{xq_w}{k_f(T - T_\infty)}, \quad Sh_x = \frac{xj_w}{D_B(C - C_\infty)}, \tag{16}$$

in which τ_w denotes surface shear stress, q_w the surface heat flux, and j_w the surface mass flux, i.e.,

$$\tau_w = \left[\nu\left(\frac{\partial u}{\partial y}\right) - \Omega\left(u\frac{\partial^2 u}{\partial x \partial y} - 2\frac{\partial u}{\partial x}\frac{\partial u}{\partial y}\right)\right]_{y=0}, \\ q_w = -k_f\left(1 + \frac{4}{3}\frac{4\sigma^* T_\infty^3}{k_f k^*}\right)\left(\frac{\partial T}{\partial y}\right)_{y=0}, j_w = -D_B\left(\frac{\partial C}{\partial y}\right)_{y=0}. \tag{17}$$

In dimensionless form, the skin friction coefficient C_{f_x}, local Nusselt Nu_x, and Sherwood Sh_x numbers are

$$\frac{1}{2}\mathrm{Re}_x^{0.5}C_{f_x} = \left[1 + \alpha f''(0)\right]f''(0), \mathrm{Re}_x^{-0.5}Nu_x = B_t\left(1 + \frac{4}{3}R\right)\left(1 + \frac{1}{\theta(0)}\right), \\ \mathrm{Re}_x^{-0.5}Sh_x = B_c\left(1 + \frac{1}{\phi(0)}\right), \tag{18}$$

in which $\mathrm{Re}_x = \frac{u_w x}{\nu}$ denotes the local Reynolds number.

3. Solutions expressions

Initial guesses (f_0, θ_0, ϕ_0) and auxiliary linear operators $(\mathscr{L}_f, \mathscr{L}_\theta, \mathscr{L}_\phi)$ for the homotopic expressions are

$$f_0(\eta) = A^*\eta + (1 - A^*)[1 - \exp(-\eta)], \quad \theta_0(\eta) = \left(\frac{B_t}{1 - B_t}\right)\exp(-\eta), \\ \phi_0(\eta) = \left(\frac{B_c}{1 - B_c}\right)\exp(-\eta), \tag{19}$$

$$\mathscr{L}_f(f) = \frac{d^3 f}{d\eta^3} - \frac{df}{d\eta}, \quad \mathscr{L}_\theta(\theta) = \frac{d^2\theta}{d\eta^2} - \theta \text{ and } \mathscr{L}_\phi(\phi) = \frac{d^2\phi}{d\eta^2} - \phi, \tag{20}$$

with the associated properties

$$\mathscr{L}_f[\Gamma_1 + \Gamma_2\exp(-\eta) + \Gamma_3\exp(\eta)] = 0, \tag{21}$$

$$\mathscr{L}_\theta[\Gamma_4\exp(-\eta) + \Gamma_5\exp(\eta)] = 0, \tag{22}$$

$$\mathscr{L}_\phi[\Gamma_6\exp(-\eta) + \Gamma_7\exp(\eta)] = 0. \tag{23}$$

Following the procedure of [39,40] one obtains

$$f_m(\eta) = f_m^\star(\eta) + \Gamma_1 + \Gamma_2\exp(-\eta) + \Gamma_3\exp(\eta), \tag{24}$$

$$\theta_m(\eta) = \theta_m^\star(\eta) + \Gamma_4\exp(-\eta) + \Gamma_5\exp(\eta), \tag{25}$$

$$\phi_m(\eta) = \phi_m^\star(\eta) + \Gamma_6\exp(-\eta) + \Gamma_7\exp(\eta). \tag{26}$$

where $f_m^\star(\eta)$, $\theta_m^\star(\eta)$, and $\phi_m^\star(\eta)$ are the special solutions and Γ_i $(i = 1 - 7)$ are the arbitrary constants given by

$$\Gamma_1 = -\left.\frac{\partial f_m^{\star}(\eta)}{\partial \eta}\right|_{\eta=0} - f_m^{*}(0), \Gamma_2 = \left.\frac{\partial f_m^{\star}(\eta)}{\partial \eta}\right|_{\eta=0}, \Gamma_3 = 0,$$
$$\Gamma_4 = \frac{1}{1-B_t}\left[\left.\frac{\partial \theta_m^{\star}(\eta)}{\partial \eta}\right|_{\eta=0} + B_t \theta_m^{\star}(0)\right], \Gamma_5 = 0, \quad (27)$$
$$\Gamma_6 = \frac{1}{1-B_c}\left[\left.\frac{\partial \phi_m^{\star}(\eta)}{\partial \eta}\right|_{\eta=0} + B_c \phi_m^{\star}(0)\right], \Gamma_7 = 0.$$

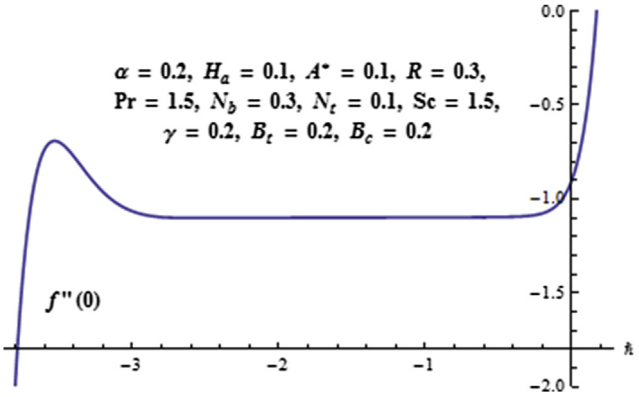

Fig. 2. $\hbar$-curve for function $f(\eta)$.

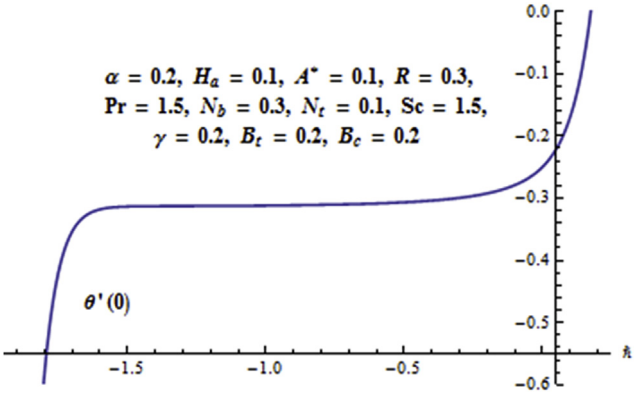

Fig. 3. $\hbar$-curve for function$\theta(\eta)$.

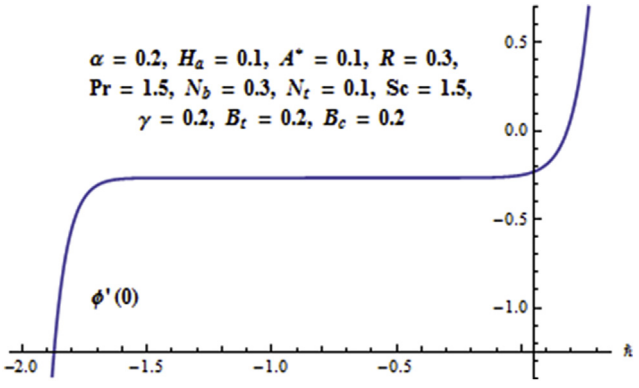

Fig. 4. $\hbar$-curve for function $\phi(\eta)$.

3.1. Convergence analysis

Construction of the series solutions by the homotopy analysis technique involves convergence control variables $\hbar_f$, $\hbar_\theta$, and $\hbar_\phi$. These convergence control variables are adequate in adjusting and controlling the convergence region of the series solutions. We plot the $\hbar$-curves to the 19th order of approximation. Admissible values are obtained by the flat portions of the $\hbar$-curves. Figs. 2–4 show that the acceptable ranges of $\hbar_f$, $\hbar_\theta$, and $\hbar_\phi$ are $-2.35 \le \hbar_f \le -0.15$, $-1.55 \le \hbar_\theta \le -0.5$, and. $-1.65 \le \hbar_\phi \le -0.2$.

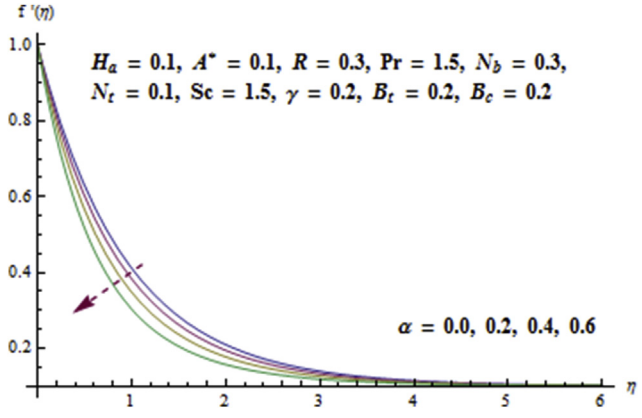

Fig. 5. $f'(\eta)$ variation via α.

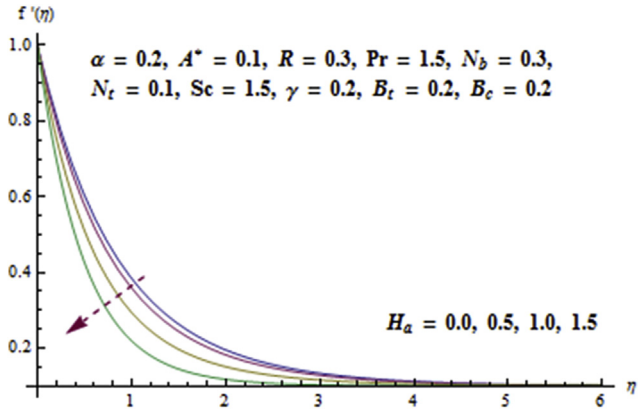

Fig. 6. $f'(\eta)$ variation via H_a.

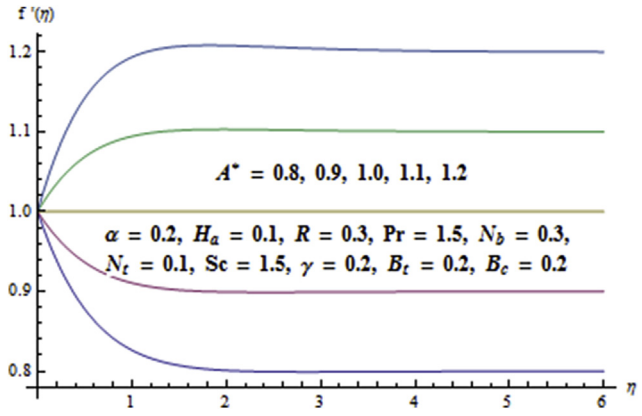

Fig. 7. $f'(\eta)$ variation via A.

3.2. Discussion

This subsection aims to investigate the characteristics of sundry physical variables on the velocities, temperature, and nanoparticle concentration. Variations in velocity fields for various values of viscoelastic parameter α, magnetic parameter H_a, and ratio parameter A are addressed in Figs. 5–7. The effect of the viscoelastic parameter α on the velocity is examined in Fig. 5. The velocity and related layer thickness decrease for larger α. In fact, higher α enhances viscoelasticity through tensile stress (which resists the boundary layer) and subsequently velocity diminishes. The effect of the magnetic parameter H_a on the velocity is described in Fig. 6. Here, both velocity and layer thickness are diminished via larger H_a. In fact, for higher values of magnetic parameter, the Lorentz force strengthens, creating more resistance to liquid motion and thus reducing the velocity. Velocity for the ratio parameter A is drawn in Fig. 7. Both the velocity and momentum layer are enhanced when $A<1$. For $A>1$ the situation is reversed. Moreover for $A=1$ no boundary layer exists.

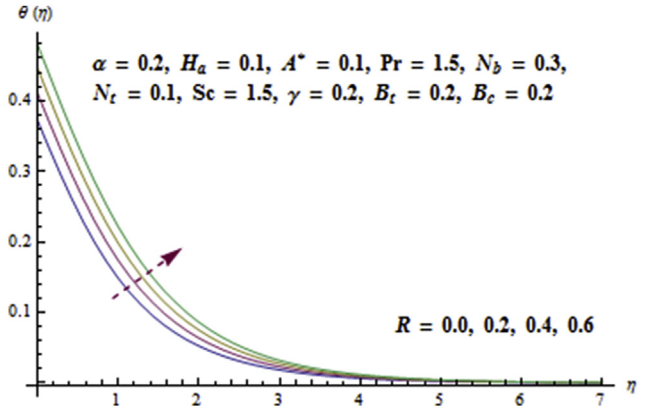

Fig. 8. $\theta(\eta)$ variation via R.

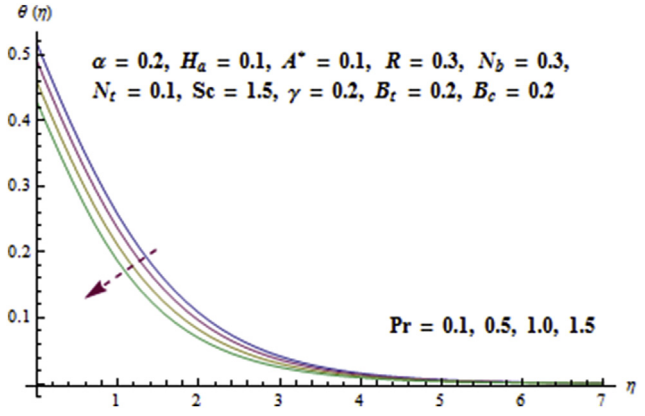

Fig. 9. $\theta(\eta)$ variation via Pr.

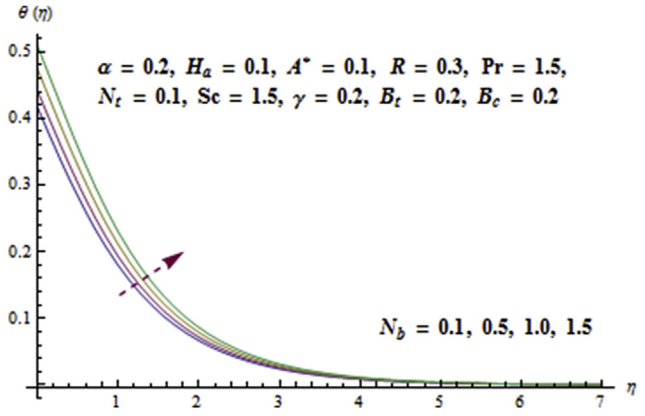

Fig. 10. $\theta(\eta)$ variation via N_b.

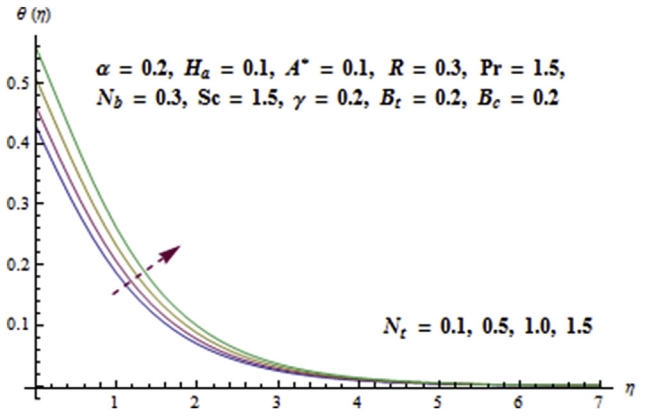

Fig. 11. $\theta(\eta)$ variation via N_t.

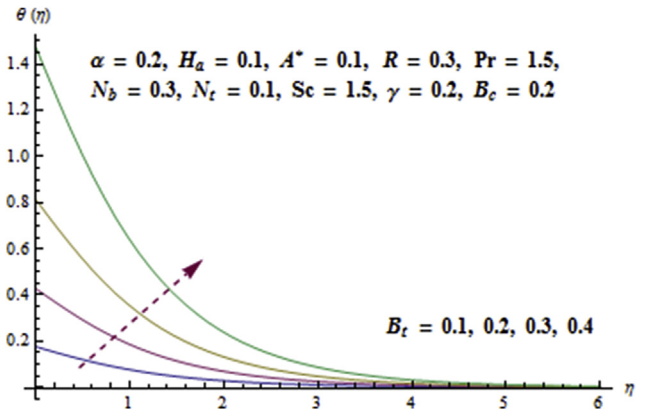

Fig. 12. $\theta(\eta)$ variation via B_t.

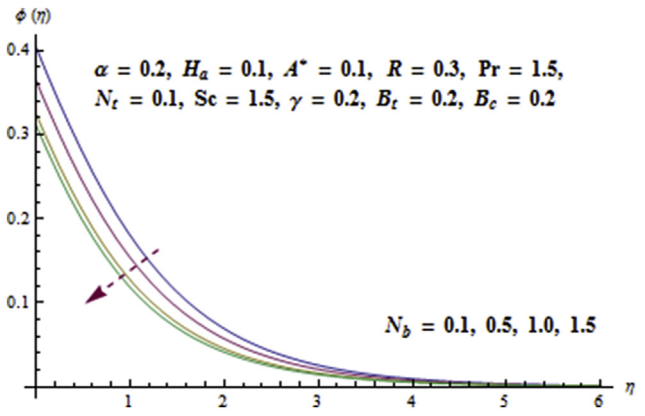

Fig. 13. $\phi(\eta)$ variation via N_b.

Influences of the radiation parameter R, Prandtl number Pr, Brownian motion parameter N_b, thermophoresis parameter N_t, and thermal conjugate parameter B_t on the temperature distributions are demonstrated in Figs. 8–12. Fig. 8 presents the effect of the radiation parameter R on the temperature field. Larger R leads to an enhancement of the temperature and thermal layer. Here, heat is produced from the radiation processes in the working fluid so the temperature field increases. The influence of the Prandtl number Pr on the temperature is depicted in Fig. 9. Decreases in the temperature and thermal layer thickness have been observed when the Prandtl number increases. The Prandtl number correlates with momentum to the thermal diffusivities; hence, higher values of Pr lead to lower thermal diffusivity, which causes decay in the temperature field. Fig. 10 demonstrates the features of the Brownian motion parameter N_b on temperature. There is an enhancement of the temperature and thermal layer thickness via N_b. In fact, more heat is produced through the random motion of fluid particles within the frame of larger Brownian motion parameter N_b. Therefore, temperature increases. Fig. 11 clearly depicts that temperature and associated layer thickness are increased for a larger thermophoresis parameter N_t. In thermophoresis, heated particles are pulled away from the hot surface to the cold region. Due to this fact, the fluid temperature rises. Fig. 12 delineates the variation of temperature for changes in the thermal conjugate parameter B_t. Both the temperature and layer thickness are an increasing function of B_t. The thermal conjugate parameter depends on the heat transfer coefficient h_t. Increasing B_t shows an increase in the heat transfer coefficient h_t, which corresponds to more heat transfer from the heated surface to the cooled surface of the fluid. This

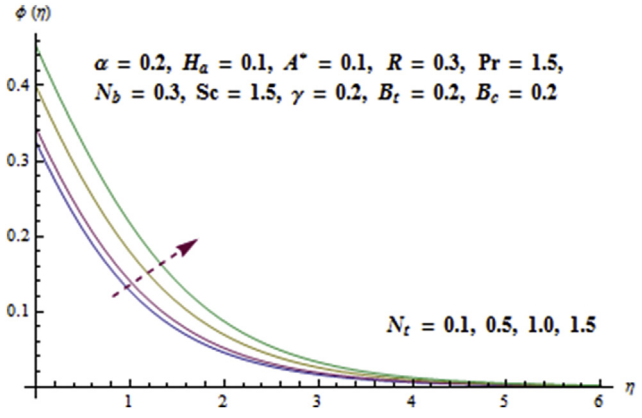

Fig. 14. $\phi(\eta)$ variation via N_t.

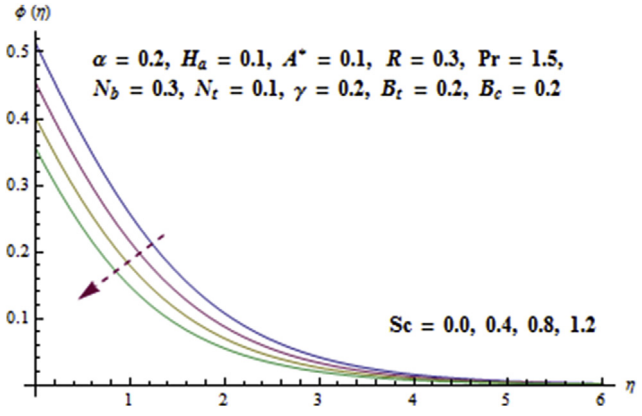

Fig. 15. $\phi(\eta)$ variation via Sc.

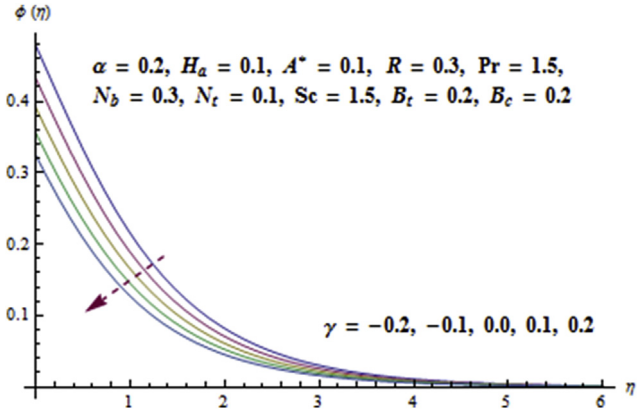

Fig. 16. $\phi(\eta)$ variation via γ.

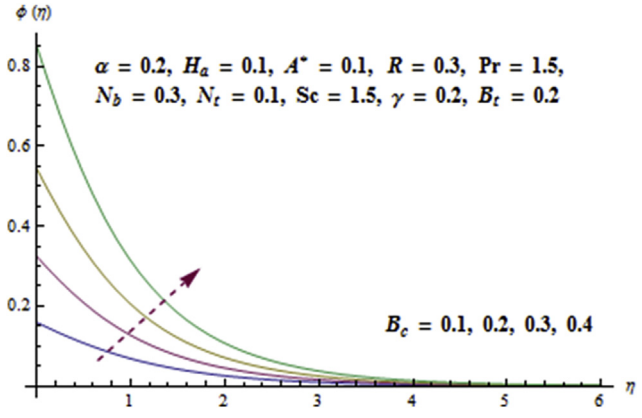

Fig. 17. $\phi(\eta)$ variation via B_c.

Table 1
Convergence when $\alpha = 0.2, H_a = 0.1, A^* = 0.1, R = 0.3, \mathrm{Pr} = 1.5, N_b = 0.3, N_t = 0.1, Sc = 1.5, \gamma = 0.2, B_t = 0.2$, and $B_c = 0.2$.

Order of approximation	$-f''(0)$	$-\theta'(0)$	$-\phi'(0)$
1	0.9999	0.2710	0.2621
5	1.0901	0.2973	0.2662
10	1.0958	0.3066	0.2662
15	1.0974	0.3101	0.2662
21	1.0984	0.3119	0.2662
25	1.0984	0.3119	0.2662
30	1.0984	0.3119	0.2662
35	1.0984	0.3119	0.2662

Table 2
Skin friction coefficient $\frac{1}{2}\mathrm{Re}_x^{0.5}C_{f_x}$ when $R = 0.3, \mathrm{Pr} = 1.5, N_b = 0.3, N_t = 0.1, Sc = 1.5, \gamma = 0.2, B_t = 0.2$, and $B_c = 0.2$.

Parameters (fixed values)	Parameters		$-\frac{1}{2}\mathrm{Re}_x^{0.5}C_{f_x}$
$H_a = 0.1, A^* = 0.1$	α	0.1	1.1321
		0.2	1.3188
		0.3	1.5346
$\alpha = 0.2, A^* = 0.1$	H_a	0.1	1.3188
		0.2	1.3337
		0.5	1.4478
$\alpha = 0.2, H_a = 0.1$	A^*	0.1	1.3188
		0.2	1.2644
		0.5	0.9747

means that the temperature of the whole liquid increases, transferring more heat from the sheet to the fluid.

The effects of the Brownian motion parameter N_b, the thermophoresis parameter N_t, the Schmidt number Sc, generative/destructive chemical reaction γ, and solutal conjugate parameters B_c on the nanoparticle concentration are inspected in Figs. 13–17. Fig. 13 offers a graphical illustration for concentration against N_b. One can see that concentration and associated layer thickness are decreased via larger N_b. For a larger Brownian motion parameter N_b, the number of collisions of the fluid particles increases, which corresponds to decay in the concentration field. It is revealed that the concentration and related layer thickness are increased for a larger thermophoresis parameter, N_t (see Fig. 14). The fluid thermal conductivity enhances in the frame of the nanoparticles. Higher N_t gives rise to the thermal conductivity of fluid. Higher thermal conductivity shows that the concentration rises. Concentrations for Sc are captured in Fig. 15. Here concentration diminishes in view of Sc. Physically the Schmidt number is the momentum to mass diffusivities ratio. For enhancement of the Schmidt number the mass diffusivity diminishes, which is responsible for the reduction of the concentration. The characteristics of generative/destructive chemical reaction γ on concentration are outlined in Fig. 16. There is an enhancement in fluid concentration in view of the destructive chemical reaction variable $(\gamma > 0)$. However, the reverse situation is noticed for the generative chemical reaction $(\gamma < 0)$. Fig. 17 provides analysis of the variation of concentration profile via the solutal conjugate parameter B_c. Both concentration and associated boundary layer thickness have increasing behavior for B_c. Since the

Table 3
Local Nusselt number $Re_x^{-0.5}Nu_x$ when $H_a = 0.1$, $Sc = 1.5$, and.$\gamma = 0.2$.

Parameters (fixed values)	Parameters		$Re_x^{-0.5}Nu_x$
$A^* = 0.1, R = 0.3, \mathrm{Pr} = 1.5, N_b = 0.3, N_t = 0.1, B_t = 0.2, B_c = 0.2$	α	0.1	0.7928
		0.2	0.7786
		0.5	0.7455
$\alpha = 0.2, R = 0.3, \mathrm{Pr} = 1.5, N_b = 0.3, N_t = 0.1, B_t = 0.2, B_c = 0.2$	A^*	0.1	0.7786
		0.2	0.8011
		0.5	0.8956
$\alpha = 0.2, A^* = 0.1, \mathrm{Pr} = 1.5, N_b = 0.3, N_t = 0.1, B_t = 0.2, B_c = 0.2$	R	0.1	0.7033
		0.3	0.7786
		0.5	0.8497
$\alpha = 0.2, A^* = 0.1, R = 0.3, N_b = 0.3, N_t = 0.1, B_t = 0.2, B_c = 0.2$	Pr	1.0	0.6529
		1.5	0.7786
		2.0	0.9108
$\alpha = 0.2, A^* = 0.1, R = 0.3, \mathrm{Pr} = 1.5, N_t = 0.1, B_t = 0.2, B_c = 0.2$	N_b	0.3	0.7786
		0.4	0.7629
		0.7	0.7212
$\alpha = 0.2, A^* = 0.1, R = 0.3, \mathrm{Pr} = 1.5, N_b = 0.3, B_t = 0.2, B_c = 0.2$	N_t	0.1	0.7786
		0.2	0.7622
		0.5	0.6899
$\alpha = 0.2, A^* = 0.1, R = 0.3, \mathrm{Pr} = 1.5, N_b = 0.3, N_t = 0.1, B_c = 0.2$	B_t	0.2	0.7786
		0.4	0.7888
		0.6	0.8412
$\alpha = 0.2, A^* = 0.1, R = 0.3, \mathrm{Pr} = 1.5, N_b = 0.3, N_t = 0.1, B_t = 0.2$	B_c	0.2	0.7786
		0.4	0.7187
		0.6	0.5869

Table 4
Local Sherwood number $Re_x^{-0.5}Sh_x$ when $H_a = 0.1$, $R = 0.3$, and.$\mathrm{Pr} = 1.5$.

Parameters (fixed values)	Parameters		$\mathrm{Re}_x^{-0.5}Sh_x$
$A^* = 0.1, N_b = 0.3, N_t = 0.1, Sc = 1.5, \gamma = 0.2, B_t = 0.2, B_c = 0.2$	α	0.1	0.8095
		0.2	0.8036
		0.5	0.7752
$\alpha = 0.2, N_b = 0.3, N_t = 0.1, Sc = 1.5, \gamma = 0.2, B_t = 0.2, B_c = 0.2$	A^*	0.1	0.8036
		0.2	0.8137
		0.5	0.8624
$\alpha = 0.2, A^* = 0.1, N_t = 0.1, Sc = 1.5, \gamma = 0.2, B_t = 0.2, B_c = 0.2$	N_b	0.3	0.8036
		0.4	0.8298
		0.7	0.8694
$\alpha = 0.2, A^* = 0.1, N_b = 0.3, Sc = 1.5, \gamma = 0.2, B_t = 0.2, B_c = 0.2$	N_t	0.1	0.8036
		0.2	0.7193
		0.5	0.5798
$\alpha = 0.2, A^* = 0.1, N_b = 0.3, N_t = 0.1, \gamma = 0.2, B_t = 0.2, B_c = 0.2$	Sc	1.0	0.6483
		1.5	0.8036
		2.0	0.9509
$\alpha = 0.2, A^* = 0.1, N_b = 0.3, N_t = 0.1, Sc = 1.5, B_t = 0.2, B_c = 0.2$	γ	0.2	0.8036
		0.4	0.9528
		0.6	1.0859
$\alpha = 0.2, A^* = 0.1, N_b = 0.3, N_t = 0.1, Sc = 1.5, \gamma = 0.2, B_c = 0.2$	B_t	0.2	0.8036
		0.4	0.5839
		0.6	0.2079
$\alpha = 0.2, A^* = 0.1, N_b = 0.3, N_t = 0.1, Sc = 1.5, \gamma = 0.2, B_t = 0.2$	B_c	0.2	0.8036
		0.4	0.8786
		0.6	0.9091

coefficient of mass transfer h_c enhances via larger solutal conjugate parameter B_c, the concentration increases.

Convergence solutions of momentum, energy, and concentration expressions are explored in Table 1. Analysis shows that computations are enough for 21st-order iterations for momentum and energy equations while fifth-order iterations of the concentration equation are sufficient for the convergent series solutions. Table 2 interprets behavior of variables on the skin friction coefficient. Here we see that increasing values of the viscoelastic parameter α and magnetic parameter H_a lead to an enhancement in the skin friction coefficient. However, it shows decreasing behavior for ratio parameter A^*. The effects of sundry variables on the local Nusselt number are expressed in Table 3. The local Nusselt number is an increasing function of ratio parameter A^*, radiation parameter R, Prandtl number Pr, and thermal conjugate parameter B_t. The local Nusselt number decreases via the Brownian motion parameter N_b, thermophoresis variable N_t, and solutal conjugate parameters B_c. Table 4 is presented to analyze the effect of sundry physical variables on the local Sherwood number. It is recognized that the Sherwood number enhances via the ratio parameter A^*, Brownian motion variable N_b, Schmidt number Sc, chemical reaction γ, and solutal conjugate parameters B_c while it diminished in view of the viscoelastic parameter α, thermophoresis variable N_t, and thermal conjugate parameter. B_t.

4. Conclusions

MHD stagnation point flow of Walter-B nanofluid over a permeable stretching sheet with heat and mass Newtonian heating has been discussed. Major highlights of the flow analysis are as follows:

1. Reduction in the velocity and thickness of the boundary layer is observed for viscoelastic parameter α.
2. Temperature and layer thickness increase via larger thermal conjugate parameter B_t.
3. The concentration field is reversed for $\gamma > 0$ and $\gamma < 0$.
4. The qualitative behavior of temperature and concentration are reversed when N_b is increased.
5. Variation of ratio parameter A^* results in the enhancement of the skin friction coefficient.
6. The behavior of local Nusselt and Sherwood numbers are opposite for N_t, B_t, and B_c.
7. The present analysis corresponds to the hydrodynamic situation when $H_a = 0$.
8. The involved physical phenomena have potential applications in nuclear safety, microreactors, nuclear reactions, etc.

Conflicts of interest

All authors have no conflicts of interest to declare.

References

[1] S. Choi, Enhancing thermal conductivity of fluids with nanoparticle. In: Siginer, D. A., Wang, H. P. (Eds.), Developments and Applications of Non-Newtonian Flows, MD-vol. 231/FED-vol. 66. ASME, New York, 99–105.

[2] J. Buongiorno, Convective transport in nanofluids, J. Heat Transfer Trans. ASME 128 (2006) 240–250.

[3] C. Zhang, L. Zheng, X. Zhang, G. Chen, MHD flow and radiation heat transfer of nanofluids in porous media with variable surface heat flux and chemical reaction, Appl. Math. Model 39 (2015) 165–181.

[4] S. Nadeem, R.U. Haq, Z.H. Khan, Numerical study of MHD boundary layer flow of a Maxwell fluid past a stretching sheet in the presence of nanoparticles, J. Taiwan Instit. Chemi. Eng. 45 (2014) 121–126.

[5] R.U. Haq, S. Nadeem, Z.H. Khan, N.S. Akbar, Thermal radiation and slip effects on MHD stagnation point flow of nanofluid over a stretching sheet, Physica E Low-Dimens. Syst. Nanostruct 65 (2015) 17–23.

[6] B.J. Gireesha, R.S.R. Gorla, B. Mahanthesh, Effect of suspended nanoparticles on three-dimensional MHD flow, heat and mass transfer of radiating Eyring-Powell fluid over a stretching sheet, J. Nanofluids 4 (2015) 474–484.

[7] B. Mahanthesh, B.J. Gireesha, R.S.R. Gorla, F.M. Abbasi, S.A. Shehzad, Numerical solutions for magnetohydrodynamic flow of nanofluid over a bidirectional non-linear stretching surface with prescribed surface heat flux boundary, J. Magn. Magn. Mater. 417 (2016) 189–196.

[8] M. Mustafa, J.A. Khan, T. Hayat, A. Alsaedi, Buoyancy effects on the MHD nanofluid flow past a vertical surface with chemical reaction and activation energy, Int. J. Heat Mass Transf. 108 (2017) 1340–1346.

[9] T. Hayat, S. Qayyum, S.A. Shehzad, A. Alsaedi, Simultaneous effects of heat generation/absorption and thermal radiation in magnetohydrodynamics (MHD) flow of Maxwell nanofluid towards a stretched surface, Results Phys. 7 (2017) 562–573.

[10] X. Si, H. Li, L. Zheng, Y. Shen, X. Zhang, A mixed convection flow and heat transfer of pseudo-plastic power law nanofluids past a stretching vertical plate, Int. J. Heat Mass Transf. 105 (2017) 350–358.

[11] S.T. Hussain, R.U. Haq, Z.H. Khan, S. Nadeem, Water driven flow of carbon nanotubes in a rotating channel, J. Mol. Liq. 214 (2016) 136–144.

[12] R.U. Haq, N.F.M. Noor, Z.H. Khan, Numerical simulation of water based magnetite nanoparticles between two parallel disks, Adv. Pow. Tech. 27 (2016) 1568–1575.

[13] K. Hsiao, Stagnation electrical MHD nanofluid mixed convection with slip boundary on a stretching sheet, Appl. Thermal Eng. 98 (2016) 850–861.

[14] B. Mahanthesh, F. Mabood, B.J. Gireesha, R.S.R. Gorla, Effects of chemical reaction and partial slip on the three dimensional flow of a nanofluid impinging on an exponentially stretching surface, Eur. Phys. J. Plus 132 (2017) 113.

[15] B. Mahanthesh, B.J. Gireesha, R.S.R. Gorla, Heat and mass transfer effects on the mixed convective flow of chemically reacting nanofluid past a moving/stationary vertical plate, Alex. Eng. J. 55 (2016) 569–581.

[16] T. Hayat, S. Qayyum, A. Alsaedi, S.A. Shehzad, Nonlinear thermal radiation aspects in stagnation point flow of tangent hyperbolic nanofluid with double diffusive convection, J. Mol. Liq. 223 (2016) 969–978.

[17] T. Hayat, S. Qayyum, M. Imtiaz, A. Alsaedi, Comparative study of silver and copper water nanofluids with mixed convection and nonlinear thermal radiation, Int. J. Heat Mass Transf. 10 (2016) 723–732.

[18] S.A. Shehzad, Z. Abdullah, F.M. Abbasi, T. Hayat, A. Alsaedi, Magnetic field effect in three-dimensional flow of an Oldroyd-B nanofluid over a radiative surface, J. Magn. Magn. Mater. 399 (2016) 97–108.

[19] D.W. Beard, K. Walters, Elastico-viscous boundary layer flows, Proc. Cambridge Philos. Soc. 60 (1964) 667–674.

[20] M.M. Nandeppanavar, M.S. Abel, J. Tawade, Heat transfer in a Walter's liquid B fluid over an impermeable stretching sheet with non-uniform heat source/sink and elastic deformation, Commun. Nonlinear Sci. Numer. Simulat. 15 (2010) 1791–1802.

[21] A.K.A. Hakeem, N.V. Ganesh, B. Ganga, Effect of heat radiation in a Walter's liquid B fluid over a stretching sheet with non-uniform heat source/sink and elastic deformation, J. King Saud Uni. Eng. Sci. 26 (2014) 168–175.

[22] T. Hayat, S. Asad, M. Mustafa, H.H. Alsulami, Heat transfer analysis in the flow of Walters-B fluid with a convective boundary condition, Chin. Phys. B 23 (2014) 084701.

[23] M. Javed, T. Hayat, M. Mustafa, B. Ahmad, Velocity and thermal slip effects on peristaltic motion of Walters-B fluid, Int. J. Heat Mass Transf. 96 (2016) 210–217.

[24] T. Hayat, S. Qayyum, A. Alsaedi, B. Ahmad, Magnetohydrodynamic (MHD) nonlinear convective flow of Walters-B nanofluid over a nonlinear stretching sheet with variable thickness, Int. J. Heat Mass Transf. 110 (2017) 506–514.

[25] O.D. Makinde, Computational modelling of MHD unsteady flow and heat transfer toward a flat plate with Navier slip and Newtonian heating, Braz. J. Chem. Eng. 29 (2012) 159–166.

[26] S.A. Shehzad, T. Hayat, M.S. Alhuthali, S. Asghar, MHD three-dimensional flow of Jeffrey fluid with Newtonian heating, J. Cent. South Uni. 21 (2014) 1428–1433.

[27] M. Ramzan, M. Farooq, W. Cui, T. Hayat, Three dimensional flow of an Oldroyd-B fluid with Newtonian heating, Int. J. Heat Fluid Flow 25 (2015) 68–85.

[28] T. Hayat, G. Bashir, M. Waqas, A. Alsaedi, MHD flow of Jeffrey liquid due to a nonlinear radially stretched sheet in presence of Newtonian heating, Result Phys. 6 (2016) 817–823.

[29] S. Liao, Homotopy analysis method in nonlinear differential equations, Springer & Higher Education Press, 2012.

[30] T. Hayat, M. Sajid, I. Pop, Three-dimensional flow over a stretching surface in a viscoelastic fluid, Nonlinear Anal. Real World Appl. 9 (2008) 1811–1822.

[31] Z. Ziabakhsh, G. Domairry, H. Bararnia, Analytical solution of non-Newtonian micropolar fluid flow with uniform suction/blowing and heat generation, J. Taiwan Inst. Chem. Eng. 40 (2009) 443–451.

[32] S.M. Moghimi, G. Domairry, S. Soleimani, E. Ghasemi, H. Bararnia, Application of homotopy analysis method to solve MHD Jeffery-Hamel flows in non-parallel walls, Adv. Eng. Software 42 (2011) 108–113.

[33] M. Waqas, M. Farooq, M.I. Khan, A. Alsaedi, T. Hayat, T. Yasmeen, Magneto-hydrodynamic (MHD) mixed convection flow of micropolar liquid due to nonlinear stretched sheet with convective condition, Int. J. Heat Mass Transf. 102 (2016) 766–772.

[34] O.A. Arqub, A. El-Ajou, Solution of the fractional epidemic model by homotopy analysis method, J. King Saud Univ. Sci. 25 (2013) 73–81.
[35] T. Hayat, S. Qayyum, A. Alsaedi, A. Shafiq, Inclined magnetic field and heat source/sink aspects in flow of nanofluid with nonlinear thermal radiation, Int. J. Heat Mass Transf. 103 (2016) 99–107.
[36] J. Sui, L. Zheng, X. Zhang, G. Chen, Mixed convection heat transfer in power law fluids over a moving conveyor along an inclined plate, Int. J. Heat Mass Transf. 85 (2015) 1023–1033.
[37] T. Hayat, S. Qayyum, A. Alsaedi, S. Asghar, Radiation effects on the mixed convection flow induced by an inclined stretching cylinder with non-uniform heat source/sink, PLoS One 12 (2017), e0175584.
[38] S. Abbasbandy, M. Yurusoy, H. Gulluce, Analytical solutions of non-linear equations of power-law fluids of second grade over an infinite porous plate, Math. Compu. App. 19 (2014) 124–133.
[39] T. Hayat, S. Qayyum, A. Alsaedi, M. Waqas, Radiative flow of tangent hyperbolic fluid with convective conditions and chemical reaction, Eur. Phys. J. Plus 131 (2016) 422.
[40] S. Qayyum, T. Hayat, A. Alsaedi, B. Ahmad, MHD nonlinear convective flow of thixotropic nanofluid with chemical reaction and Newtonian heat and mass conditions, Results Phy. 7 (2017) 2124–2133.